Hyperdirect connectivity of opercular speech network to the subthalamic nucleus

Ahmed Jorge[1,6], **Witold J. Lipski**[6], **Dengyu Wang**[2,6], **Donald J. Crammond**[6], **Robert S. Turner**[3], **R. Mark Richardson**[4,5,7,*]

[1]Department of Neurosurgery, The Ohio State University College of Medicine, Columbus, OH 43210, USA

[2]Tsinghua University School of Medicine, Beijing 100084, China

[3]Department of Neurobiology, University of Pittsburgh School of Medicine, Pittsburgh, PA 15213, USA

[4]Department of Neurosurgery, Massachusetts General Hospital, 55 Fruit Street, Boston, MA 02114, USA

[5]Harvard Medical School, Boston, MA 02115, USA

[6]Department of Neurosurgery, University of Pittsburgh School of Medicine, Pittsburgh, PA 15213, USA

[7]Lead contact

SUMMARY

How the basal ganglia participate in the uniquely human behavior of speech is poorly understood, despite their known role in modulating critical aspects of cognitive and motor behavior. The subthalamic nucleus (STN) is well positioned to facilitate basal ganglia functions critical for speech. Using electrocorticography in patients undergoing awake deep brain stimulation (DBS) surgery, evidence is reported for a left opercular hyperdirect pathway in humans via stimulating the STN and examining antidromic-evoked activity in the left temporal, parietal, and frontal opercular cortex. These high-resolution cortical and subcortical mapping data provide evidence for hyperdirect connectivity between the inferior frontal gyrus and the STN. In addition, evoked potential data are consistent with the presence of monosynaptic projections from areas of the opercular ections may be unique to humans, evolving alongside the ability for speech.

Graphical abstract

In brief

Using electrical stimulation of the subthalamic nucleus and simultaneous cortical recordings in individuals undergoing deep brain stimulation, Jorge et al. provide electrophysiological evidence for a hyperdirect pathway to the basal ganglia from cortical areas that control sensory and motor-planning aspects of speech.

INTRODUCTION

Possibly no human behavior requires more temporally precise control of multiple motor commands than speech. Speech neuroscience has traditionally focused on the cortex, but the importance of the basal ganglia in speech control is evidenced across an evolutionary scale. Genetic mutations that affect basal ganglia development result in extreme deficits in speech motor control and language comprehension (Lai et al., 2001), and damage to the adult basal ganglia can produce a variety of speech deficits (Lieberman, 2009). All regions of the basal ganglia share a common circuit plan, where the striatum receives topographically organized excitatory inputs from many cortical areas and conveys those inputs via direct and indirect pathways through the basal ganglia; this topography is largely conserved in outflow projections through the thalamus back to the cortex. Thus, distinct motor, associative, and limbic functions are mediated via parallel cortical-basal ganglia-thalamocortical loops (Alexander et al., 1986; Kelly and Strick, 2004).

Many cortical areas also send a monosynaptic "hyperdirect projection" to the subthalamic nucleus (STN) (Kelly and Strick, 2004; Nambu et al., 1996). Presence of this pathway in humans was demonstrated recently by measuring evoked potentials (EPs) in the sensorimotor cortex in response to low-frequency STN stimulation (Miocinovic et al., 2018). The recorded EPs include temporal components that group into three latency ranges: (1) very short latency (<2 ms), consistent with transcortical motor EPs (MEPs) in muscles, mediated by excitation of the corticospinal tract adjacent to the STN, (2) short latency (2–10 ms), consistent with antidromic activation of the hyperdirect pathway followed by cortico-cortical activation, and (3) long latency (10–100 ms), consistent with orthodromic cortical activation of basal ganglia-thalamocortical pathways. Although it has been hypothesized that output from the basal ganglia projects to Broca's area (Ullman, 2006) (disynaptically via the thalamus), whether the basal ganglia receive direct input from Broca's area remains uncertain. Based on Haynes and Haber's demonstration of hyperdirect projections from multiple frontal regions in non-human primates (Haynes and Haber, 2013), we hypothesized that Broca's area, the left inferior frontal gyrus, has hyperdirect connections with the STN. Among models of speech motor control, only state feedback control models (Houde and Nagarajan, 2011) (Bohland et al., 2010) devote significant attention to the function of basal ganglia-thalamocortical loops. No model of speech production, however, considers the cortico-subthalamic hyperdirect pathway for cortical input to basal ganglia.

We recently described STN single-unit and local-field-potential (LFP) activity during speech production (Chrabaszcz et al., 2019). Based on these studies and prior studies that demonstrated the functional connectivity of the STN to multiple cortical areas using simultaneous intracranial cortical-subthalamic recordings(Alhourani et al., 2015; Lipski et al., 2017), we hypothesized that cortical areas subserving not only speech production, but also perception, are connected to the STN via hyperdirect connections. Using electrocorticography (ECoG) in patients undergoing STN deep brain stimulation (DBS) implantation, we tested these hypotheses by recording cortical potentials evoked by STN stimulation and correlating their locations to the sites stimulated within the STN. This method avoids the inherent limitations of diffusion-weighted, magnetic-resonance-imaging approaches to tract tracing (Campbell and Pike, 2014; Thomas et al., 2014). We found evidence for antidromic activation of premotor and motor regions of the frontal operculum. Remarkably, we found similar evidence for antidromic activation of the sensory cortex, including auditory regions of the superior temporal gyrus. Given that no tracing studies in non-human primates, to our knowledge, have described these pathways (Emmi et al., 2020; Hartmann-Von Monakow et al., 1978; Kunzle, 1978; Winer, 2006), hyperdirect connections of the cortical opercular speech network to the STN may be uniquely human.

RESULTS

We successfully recorded and analyzed EPs from 20 patients with Parkinson's disease, 17 with STN stimulation, and 3 with globus pallidus (GP) stimulation. Cortical recording locations spanned multiple gyri, and basal ganglia stimulation locations primarily spanned the sensorimotor territories of the STN or the GP (Figures 1A–1D).

Antidromic cortical excitation

We identified 9,450 distinct mean voltage-time traces, each of which corresponded to a distinct combination of cortical ECoG recording location and STN stimulation location and amplitude. Three distinct short latency (2–10 ms) peaks related to antidromic activation were observed in each cortical region (Figure 2A), consistent with the existence of a fast-conducting monosynaptic connection. These peaks were present not only in premotor and motor regions (Chen et al., 2020; Miocinovic et al., 2018) but also in the superior marginal gyrus (SMG) and the superior temporal gyrus (STG). No distinct peaks in the 2–10 ms latency period were observed during stimulation in the GP externa (GPe) or internus (GPi), although a very short latency (<2 ms) EP0 was observed with both GPi and STN stimulations, consistent with antidromic activation of the descending corticospinal tract. Potentials evoked at long latencies (20–100 ms) were observed consistently in response to both STN and GP stimulations (see example in Figure S1). STN stimulation evoked long-latency responses at two distinct latencies (latency for the two associated peaks: 39.5 ± 0.7 and 60.1 ± 4.2 ms) irrespective of STN stimulation location. Stimulation of the GPe EPs at a longer latency (24.1 ± 0.2 and 46.3 ± 2.6 ms) than did stimulation of GPi (latency for the two associated peaks: 17.6 ± 0.1 and 38.8 ± 2.4 ms), consistent with the interpretation that long-latency potentials were mediated by orthodromic activation via the basal ganglia-thalamocortical loop (Figure S1). To quantify the average cortical evoked response in the 2–10 ms range from STN stimulation, we averaged all traces (n = 9,450) (Figure 2B). The average amplitude and latency responses were 1.8 ± 2.9 μV and 3.1 ± 0.8 ms for EP1, 1.5 ± 2.7 μV and 4.9 ± 1.3 ms for EP2, and 1.1 ± 2.3 μV and 6.5 ± 1.8 ms for EP3.

To quantify the STN stimulation threshold (and resulting EP peak magnitude), we tested the effects of different stimulation amplitudes on EP amplitude (Figure 2C) in different cortical locations (Figure S2). EP1 and EP2 amplitudes were dependent on stimulation intensity up to 3 mA ($F_{2,9085} = 1,408$, $p < 0.001$ and $F_{2,8650} = 505$, $p < 0.001$, ANOVA, respectively), while EP3 did not show variation with different stimulation amplitudes ($F_{2,7934} = 4.5$, $p = 0.11$, ANOVA). We did not test stimulations with currents higher than 3 mA, given that the average EP standard deviation with 3 mA stimulation was 2.84 μV. Stimulations of 1 and 2 mA were shown to be subthreshold, given that stimulation at 3 mA produced significantly higher EP amplitudes. Moreover, given that the average EP standard deviation with 3 mA stimulation was 2.84 μV, we decided to perform all subsequent analysis at a stimulation intensity of 3 mA. The reason we did not perform stimulations at a higher amplitude than 3 mA was to maintain recordings of robust cortical EP responses (i.e., higher than subthreshold) while minimizing voltage spread within the STN and spread to the internal capsule. In addition, as the neural basis of the circuitry, which generated the long-latency EPs, can only be speculated, we focused the analysis entirely on the EP1 component, as it is likely the only EP component arising from the activation of the hyperdirect pathway alone (Ashby et al., 2001; Chen et al., 2020; Kuriakose et al., 2010; Miocinovic et al., 2018).

Next, we investigated whether the wide range of EP1 latencies and amplitudes varied as a function of cortical location. We found that EP1 amplitude varied significantly between cortical locations ($F_{7,6146} = 210$, $p < 0.001$, ANOVA) with voltage mean and standard

deviation for the precentral (preCG; 1.9 ± 1.5 µV), middle frontal (MFG; 1.5 ± 1.5 µV), postcentral (postCG; 1.8 ± 1.4 µV), triangular part of the inferior frontal (pars T.; 1.2 ± 0.7 µV), opercular part of the inferior frontal (pars O.; 2.1 ± 1.6 µV), STG (2.0 ± 1.5 µV), sub-callosal cingulate (SCG; 2.0 ± 1.4 µV), and SMG (1.6 ± 1.3 µV) gyri shown in Figure 2D. These voltage differences suggested that different locations within the STN receive a different proportion of efferent axons from different cortical areas. A similar analysis for latency did not reveal significant differences. The stimulation voltage variance for each area exhibited a broad range of voltage amplitudes, which suggests that the nature of the hyperdirect connection also depends on the precise location within the STN.

Cortical EP amplitude depends on STN stimulation location

We observed wide EP ranges for each cortical area (Figure 2D). To better understand this variability, we separated each EP as a function of the cortical area and STN stimulation location. We found that for the preCG, the EP amplitude was a function of the STN stimulation location (Figures 3A–3C). For the preCG cortical EPs, STN stimulation locations closer to the center of the STN motor region, as defined by the DISTAL subcortical atlas, produced a significantly higher EP voltage than when stimulating closer to the center of the STN associative region (Spearman's rho = −0.53, p < 0.001). In contrast, STN stimulation closer to the STN associative region center produced higher EPs in the MFG (Figures 3D–3F) when compared with stimulations closer to the STN motor region (Spearman's rho = 0.41, p = 0.003). The estimated distance between these two centers is 2.1 mm.

By visualizing EP1 on the cortex, we found that stimulations closer to the STN motor region produced higher EP1 in cortical regions closer to the central sulcus (Figure 4A), while stimulations closer to the STN associative region produced higher EP1 in cortical regions farther away from the central sulcus (Figure 4B). In order to summarize the overall findings for STN subregions receiving input via the hyperdirect pathway, we plotted the weighted center of the average cortical EP amplitude (from Figures 3A–3F) for each cortical area onto the STN map and projected them onto the STN axis (Figures 4C–4F). We took this STN axis location and compared it with the distance from the central sulcus (a fronto-posterior simplification of the cortex). We found that there was a significant relationship between the STN location (motor to associative region) and distance from central sulcus (Spearman's rho = 0.80, p = 0.01). In other words, stimulation of the STN motor region produced the highest voltages in cortical regions closer to the central sulcus (e.g. preCG, postCG, and SCG), which strongly suggests that these cortical areas project the highest density of efferent fibers directly to innervate STN, while stimulation of STN associate regions produced the highest voltages in cortical regions further away from the central sulcus (e.g. MFG, pars T., and SMG).

DISCUSSION

We used high-density ECoG to record directly from the cortical surface in patients undergoing DBS implantation to demonstrate that all areas of the cortical opercular speech network, including sensory areas, are monosynaptically connected to the STN.

We confirmed recently reported physiological evidence of hyperdirect (monosynaptic) connectivity between the inferior frontal gyrus (IFG) and STN in humans (Chen et al., 2020) and extended those findings to include sensory cortical areas involved in speech processing. In agreement with the idea that input to the STN is segregated within topographically organized loops, with a degree of overlap, we found that stimulation closer to the central motor territory of the STN was more likely to produce EPs in cortical areas closer to the central sulcus, while stimulation closer to the associative territory of the STN was more likely to produce EPs in cortical areas further from the central sulcus.

Evidence for hyperdirect pathway projections to the opercular cortical speech network

Given that non-human primates do not speak and that viral synaptic tracing studies cannot be performed in humans, EP mapping during STN DBS surgery is the only method that can directly characterize a speech cortex to an STN hyperdirect pathway in humans. Mapping the hyperdirect pathway from speech-related cortical areas is important for several reasons: (1) these areas enable behavior that is uniquely human, and thus their connectivity to subcortical nuclei may be uniquely human; 2) the hyperdirect pathway has been proposed to administer a brake signal by stimulating GPi, yet it also may administer a GO signal by stimulating GPe, indirectly inhibiting GPi; understanding the origin of direct inputs to the STN can inform hypothesis generation regarding the functional roles of these inputs (Cai et al., 2019; Mosher et al., 2020); and 3) hyperdirect connectivity likely signifies the presence of loops that allow information in the speech-specific cortex to be transferred directly to the direct and indirect basal ganglia pathways in order to modulate speech production.

We showed the occurrence of three clusters of STN-stimulation-evoked cortical potential peaks (EP1, EP2, and EP3) in the 2–10 ms range, previously described in electroencephalogram (EEG) (Ashby et al., 2001; Baker et al., 2002; Kuriakose et al., 2010; Walker et al., 2012), ECoG (Kumaravelu et al., 2018; Miocinovic et al., 2018), magnetoencephalography (MEG) (Hartmann et al., 2018), and finite-element modeling (Anderson et al., 2018) studies as consistent with antidromic cortical activation via the hyperdirect pathway. Indeed, the latencies of these peaks were too fast (2–10 ms) to be of orthodromic origin via the GP and thalamus (a relay that has a duration on the order of 10–40 ms) and too slow to be related to corticospinal pathways (<1.5 ms, e.g., EP0) (Ashby et al., 2001; Miocinovic et al., 2018). We focused on the EP1 peak since it is putatively the most significant peak associated with the hyperdirect pathway. Although the second and third EP peaks observed could be associated with slower and less myelinated hyperdirect pathway fibers, these peaks could also be the product of cortico-cortical interactions after the first antidromic impulse, a multiphasic response from an activated GP-STN pathway (Magill et al., 2004) or the product of an STN-to-cortex direct pathway (Degos et al., 2008).

We showed that these potentials can be evoked across broad areas of the cortex. Although the majority of afferents to the STN come from the GPe, it has been argued that the hyperdirect pathway can carry key inputs to alter motor and non-motor functions mediated by the basal ganglia (Delaville et al., 2015; Magill et al., 2004; Mathai and Smith, 2011; Nambu et al., 2002). In addition, computational models have shown that DBS stimulation can robustly propagate signals to the motor cortex with high fidelity (Anderson et al.,

2018). Here, we show the involvement of other cortical areas, particularly areas involved with speech production. In agreement with our results, the left inferior frontal cortex (including pars T. and pars O.), hypothesized to part of the basal ganglia thalamocortical circuitry (Ullman, 2006), has been suggested to be directly connected to the STN by human tractography and fMRI studies (Aron et al., 2007).

STN hyperdirect pathway is topographically organized

The basal ganglia topographical organization with motor, associative, and limbic circuitry having distinct regions across the putamen, GPe, and GPi has been well described (Alexander et al., 1986; Middleton and Strick, 2000; Obeso et al., 2008). Here, we show that stimulation in the ventromedial STN produces higher EPs in the premotor cortex, while stimulation in dorsolateral STN produces higher EPs in the motor cortex, consistent with anterograde tracer and single-unit recording studies in non-human primates (Haynes and Haber, 2013). Moreover, there is a relationship between STN stimulation location and the estimated cortical EP distance from the central sulcus, suggesting a precise topography of cortical innervation of the STN. In addition to shedding light on STN function, hyperdirect-pathway topology is also of clinical importance, given that stimulation of different STN subregions has been associated with non-motor behavioral responses, in patients with Parkinson's disease (PD) (Akram et al., 2017; Mallet et al., 2007).

Rapid modulation of the control of speech requires highly co-ordinated information transfer between the planning, production, and perception hubs of the speech network. Hyperdirect connectivity of premotor, motor-sensory, and auditory cortical regions suggests that the basal ganglia may play an integral role in state feedback control of speech production, where auditory information is compared with a prediction derived from an efference copy of motor output (Houde and Nagarajan, 2011). The basal ganglia are well suited to modulate these processes (Bohland et al., 2010; Civier et al., 2013) and have been implicated in the processing of prediction errors (Lardeux et al., 2013; Lau et al., 2017; Siman-Tov et al., 2019), which in the context of speech production would contribute to an internal model tracking the state of the vocal tract. In addition to a potential role in evaluating efference copy, the STN could participate in speech gain modulation (Chrabaszcz et al., 2019; Turner and Desmurget, 2010) via either movement inhibition or a prokinetic effect (Fischer et al., 2017). The relay of auditory information directly to the STN could help shape this modulation. Indeed, we have previously shown evidence for an indirect information flow between the primary sensory cortex and the STN during hand-gripping movements (Alhourani et al., 2020; Lipski et al., 2017). The existence of a sensory hyperdirect pathway, however, has not previously been hypothesized. Studies in rat models (Kolomiets et al., 2001; Magill et al., 2004), stimulating the cortex and measuring spikes and LFPs evoked in the basal ganglia, have shown evidence for the existence of hyperdirect projections to the STN from prefrontal, premotor, cingulate, M1, and S1 and the absence of such a projection from the auditory cortex. In contrast, a tractography study in humans did suggest the presence of a hyperdirect connection from prefrontal, M1, S1, and STG to the STN (Brunenberg et al., 2012). It is possible, therefore, that hyperdirect connections to STN from sensory cortical areas, ultimately involved in processes related to speech perception, have co-evolved with speech ability in humans.

Conclusion

By combining intracranial recordings from the basal ganglia and focal electrical stimulation of the cortex in subjects undergoing DBS, this study expands the known monosynaptic cortical inputs to the human STN to include the entire frontal-parietal-temporal opercular cortex, including the auditory cortex. These data provide evidence for a hyperdirect pathways from motor planning, motor sensory, and auditory sensory cortices to the basal ganglia that are uniquely positioned to participate in speech production.

Limitations of the study

We tested stimulation amplitudes in the 1–3 mA range (see Figure S2) since the variance of the EP at 3 mA became large. The magnitude of EPs did not reach an asymptote suprathreshold within this range of stimulation currents, however, and thus we cannot be certain that 100% of the hyperdirect efferents were activated. We understand that the EP amplitude represents the amplitude of the net dipole summed over thousands of local dipoles in the region covered by our ECoG grid. We assumed that all local dipoles were sampled evenly across all the available cortical coverage as shown in Figure 1; we are not taking into consideration dipoles occurring outside the ECoG coverage area or dipoles in sulcal depths (due to an inherent lack of ECoG coverage). Of note, given the number of contacts and multiple area comparisons, we may not have had adequate statistical power to detect significant differences in EP latencies, where trends were observed.

STAR★METHODS

RESOURCE AVAILABILITY

Lead contact—Further information and requests for data and code should be directed to and will be fulfilled by the lead contact, Mark Richardson (mark.richardson@mgh.harvard.edu).

Materials availability—This study did not generate new unique reagents.

Data and code availability—Data will be available through DABI (Data Archive BRAIN Initiative), a shared repository for invasive neurophysiology data from the NIH Brain Research Through Advancing Innovative Neurotechnologies (BRAIN) Initiative. In addition, the data have been uploaded to Harvard Dataverse (https://doi.org/10.7910/DVN/CNI25V). The code has been uploaded to Github (https://doi.org/10.5281/zenodo.5932678; https://zenodo.org/record/5932678#.Yfhus2BOkh8).

Any additional information required to reanalyze the data reported in this paper is available from the lead contact upon request.

EXPERIMENTAL MODEL AND SUBJECT DETAILS

Participants and surgery—Twenty patients undergoing STN (n = 17), globus pallidus internus (GPi, n = 3) DBS surgery for Parkinson's disease were enrolled in an IRB-approved protocol, following informed consent. All patients were right-handed with presumed left language dominance. Dopaminergic medications were held for 12 h prior to surgery. The

STN or GPi was targeted utilizing standard clinical techniques in awake, microelectrode-guided surgery (Faraji et al., 2020; Lee et al., 2018). It was the surgeon's practice to always begin with the left side first, and all data were collected in the left hemisphere. Prior to insertion of microelectrodes, one or two subdural high-density ECoG arrays (63 channels, 1 mm contact diameter, 3 mm separation, 3×21 contact configuration; PMT, Chanhassen, MN, USA) were temporarily placed at prespecified cortical locations through the single standard burr hole. The ECoG Strip location was planned preoperatively to span cortical areas including the frontal operculum and/or the premotor, ventral sensorimotor, and superior temporal cortex.

METHOD DETAILS

STN/GPi stimulation and ECoG recordings—Sedation was held and patients were at their neurological baseline as assessed by clinical examination, prior to the onset of clinical microelectrode recording. Clinical microelectrode recording was completed using three simultaneously placed Alpha Omega Microprobe electrodes (Alpha Omega Co, Alpharetta, GA, USA) in the center, medial, and posterior trajectories of the Ben-Gun array. STN or GPi monopolar stimulation was conducted for clinical mapping purposes through the macro cylindrical contact ("ring electrode", diameter 0.7 mm, length 1 mm) using the Neuro Omega (Alpha Omega Co, Alpharetta, GA, USA) stimulation software. Upon completion of clinical testing, monitored anesthesia had been held for least 45 min. Research stimulation then was conducted at 1Hz for 30 s (30 stimulation pulses) or 10 Hz for 30 s (300 stimulation pulses) at stimulation intensities of 1, 2 and 3 mA, at two separate depths within the STN, separated by at least 2 mm in the z-dimension. Simultaneous with stimulation, cortical evoked potentials were recorded, amplified, and digitized using a Grapevine Neural Interface Processor (Ripple Neuro, Salt Lake City, UT, USA). Signals were recorded at sampling rate of 10 kHz with all channels referenced to scalp ground.

Localization of ECoG recordings and STN stimulation leads—ECoG strip location was determined with intraoperative fluoroscopy imaging or CT imaging, preoperative in-frame CT, and preoperative MRI as previously described (Randazzo et al., 2016). Normalization of each subject's MRI to MNI brain space and automatic identification of ECoG electrode and gyri location was conducted a posteriori with FreeSurfer and the Destrieux atlas (Dale et al., 1999; Destrieux et al., 2010). According to this atlas, eight anatomical categories were covered by ECoG recordings in this study, including the opercular part of the inferior frontal gyrus (Pars O.), the triangular part of the inferior frontal gyrus (Pars T.), the middle frontal (MFG), precentral (PreCG), postcentral (PostCG), subcentral (SC), supramarginal (SM) and superior temporal gyrus (STG). STN contact locations were determined using Lead-DBS MNI ICBM atlas and software (Horn and Kühn, 2015). DICOM images were coregistered using Advanced Normalization Tools(ANTs) and hybrid statistical parametric mapping (SPM) algorithms and then normalized to the International Consortium for Brain Mapping (ICMB) 152 nonlinear 2009b template. Coordinates were recorded in MNI space and STN geometry (i.e. motor, associative, limbic) was defined by the DISTAL atlas (Ewert et al., 2018).

Signal preprocessing—Stimulation start times were assigned by identifying the first time-bin with largest voltage deflection on a channel displaying a large stimulation artifact. The remaining ECoG channels were aligned to these stimulation times and a trial was defined by each stimulation time. To filter out low-frequency fluctuations without introducing filter artifacts, raw voltage values for each trial were de-trended by subtracting a low-order polynomial fit of the signal (eighth order). For 1 Hz stimulation, 30 trials within each session were averaged per channel and then smoothed using a 5-bin (0.17 ms) moving window (Miocinovic et al., 2018). The first positive voltage peak deflection (peak 0) after stimulation was defined as cortical evoked potential 0 (EP0), with subsequent voltage peak deflections labeled as EP1 through EP3. Each temporal component of the evoked potential was separated into the peak and trough of each response accordingly; for example, cortical evoked potential 1 (EP1) amplitude and latency were defined as the amplitude from trough 1 (T1) to peak 1 (P1) and the latency was defined at the peak of P1. All data processing and analysis was performed using custom code in MATLAB 2017 (Mathworks, Natick, MA).

Weighted-center of cortical evoked potential calculation—To determine the location in the STN that receives the strongest hyperdirect projection from each cortical area, a weighted-center of voltage calculation was taken. This calculation is analogous to a center of mass calculation, with voltage (in our case, EP1) being the weight for each STN stimulation location. In this case, **R** is defined as the vector that points to the center of weighted EP. In other words, **R** is the location at which the STN would produce an average cortical response in the cortical area of interest based on the sum of all actual stimulation locations, $\mathbf{r}_i$, multiplied by the recorded evoked cortical responses, v_i.

$$\boldsymbol{R} = \frac{1}{V} \sum_{i=1}^{n} v_i \boldsymbol{r}_i$$

To simplify the dimensionality of the STN space, we defined a one-dimensional STN axis with two points, namely the center of the STN associative region volume (as described in [name] atlas) (MNI coordinates = [−10.4 −11.7 −7.6] mm) and center of STN motor region volume (MNI coordinates = [−12.6 −15.0 −7.1] mm) with origin at the STN center.

QUANTIFICATION AND STATISTICAL ANALYSIS

Statistical analysis—Analysis of variance (ANOVA) was performed with multiple comparison correction using the Tukey-Kramer method.

Supplementary Material

Refer to Web version on PubMed Central for supplementary material.

ACKNOWLEDGMENTS

REFERENCES

Akram H, Georgiev D, Mahlknecht P, Hyam J, Foltynie T, Limousin P, Jahanshahi M, Hariz M, Zrinzo L, Ashburner J, et al. (2017). Subthalamic deep brain stimulation sweet spots and hyperdirect cortical connectivity in Parkinson's disease. Neuroimage 158, 332–345. [PubMed: 28711737]

Alexander GE, DeLong MR, and Strick PL (1986). Parallel organization of functionally segregated circuits linking basal ganglia and cortex. Annu. Rev. Neurosci 9, 357–381. [PubMed: 3085570]

Alhourani A, McDowell MM, Randazzo MJ, Wozny TA, Kondylis ED, Lipski WJ, Beck S, Karp JF, Ghuman AS, and Richardson RM (2015). Network effects of deep brain stimulation. J. Neurophysiol 114, 2105–2117. [PubMed: 26269552]

Alhourani A, Korzeniewska A, Wozny TA, Lipski WJ, Kondylis ED, Ghuman AS, Crone NE, Crammond DJ, Turner RS, and Richardson RM (2020). Subthalamic nucleus activity influences sensory and motor cortex during force transduction. Cereb. Cortex 30, 2615–2626. [PubMed: 31989165]

Anderson RW, Farokhniaee AA, Gunalan K, Howell B, and McIntyre CC (2018). Action potential initiation, propagation, and cortical invasion in the hyperdirect pathway during subthalamic deep brain stimulation. Brain Stimul 11, 1140–1150. [PubMed: 29779963]

Aron AR, Behrens TE, Smith S, Frank MJ, and Poldrack RA (2007). Behavioral/Systems/cognitive triangulating a cognitive control network using diffusion-weighted magnetic resonance imaging (MRI) and functional MRI. J. Neurosci 27, 3743–3752. [PubMed: 17409238]

Ashby P, Paradiso G, Saint-Cyr JA, Chen R, Lang AE, and Lozano AM (2001). Potentials recorded at the scalp by stimulation near the human subthalamic nucleus. Clin. Neurophysiol 112, 431–437. [PubMed: 11222963]

Baker KB, Montgomery EB, Rezai AR, Burgess R, and Lüders HO (2002). Subthalamic nucleus deep brain stimulus evoked potentials: physiological and therapeutic implications. Mov. Disord 17, 969–983. [PubMed: 12360546]

Bohland JW, Bullock D, and Guenther FH (2010). Neural representations and mechanisms for the performance of simple speech sequences. J. Cogn. Neurosci 22, 1504–1529. [PubMed: 19583476]

Brunenberg EJL, Moeskops P, Backes WH, Pollo C, Cammoun L, Vilanova A, Janssen MLF, Visser-Vandewalle VERM, ter Haar Romeny BM, Thiran JP, et al. (2012). Structural and resting state functional connectivity of the subthalamic nucleus: identification of motor stn parts and the hyperdirect pathway. PLoS One 7, e39061. [PubMed: 22768059]

Cai W, Duberg K, Padmanabhan A, Rehert R, Bradley T, Carrion V, and Menon V (2019). Hyperdirect insula-basal-ganglia pathway and adult-like maturity of global brain responses predict inhibitory control in children. Nat. Commun 10, 1–13. [PubMed: 30602773]

Campbell JSW, and Pike GB (2014). Potential and limitations of diffusion MRI tractography for the study of language. Brain Lang 131, 65–73. [PubMed: 23910928]

Chen W, de Hemptinne C, Miller AM, Leibbrand M, Little SJ, Lim DA, Larson PS, and Starr PA (2020). Prefrontal-subthalamic hyperdirect pathway modulates movement inhibition in humans. Neuron 106, 579–588.e3. [PubMed: 32155442]

Chrabaszcz A, Neumann WJ, Stretcu O, Lipski WJ, Bush A, Dastolfo-Hromack CA, Wang D, Crammond DJ, Shaiman S, Dickey MW, et al. (2019). Subthalamic nucleus and sensorimotor cortex activity during speech production. J. Neurosci 39, 2698–2708. [PubMed: 30700532]

Civier O, Bullock D, Max L, and Guenther FH (2013). Computational modeling of stuttering caused by impairments in a basal ganglia thalamo-cortical circuit involved in syllable selection and initiation. Brain Lang 126, 263–278. [PubMed: 23872286]

Dale AM, Fischl B, and Sereno MI (1999). Cortical surface-based analysis. Neuroimage 9, 179–194. [PubMed: 9931268]

Degos B, Deniau JM, Le Cam J, Mailly P, and Maurice N (2008). Evidence for a direct subthalamo-cortical loop circuit in the rat. Eur. J. Neurosci 27, 2599–2610. [PubMed: 18547246]

Delaville C, McCoy AJ, Gerber CM, Cruz AV, and Walters JR (2015). Subthalamic nucleus activity in the awake hemiparkinsonian rat: relationships with motor and cognitive networks. J. Neurosci 35, 6918–6930. [PubMed: 25926466]

Destrieux C, Fischl B, Dale A, and Halgren E (2010). Automatic parcellation of human cortical gyri and sulci using standard anatomical nomenclature. Neuroimage 53, 1–15. [PubMed: 20547229]

Emmi A, Antonini A, Macchi V, Porzionato A, and De Caro R (2020). Anatomy and connectivity of the subthalamic nucleus in humans and non-human primates. Front. Neuroanat 14, 13. [PubMed: 32390807]

Ewert S, Plettig P, Li N, Chakravarty MM, Collins DL, Herrington TM, Kühn AA, and Horn A (2018). Toward defining deep brain stimulation targets in MNI space: a subcortical atlas based on multimodal MRI, histology and structural connectivity. Neuroimage 170, 271–282. [PubMed: 28536045]

Faraji AH, Kokkinos V, Sweat JC, Crammond DJ, and Richardson RM (2020). Robotic-assisted stereotaxy for deep brain stimulation lead implantation in awake patients. Oper. Neurosurg 19, 444–452.

Fischer P, Pogosyan A, Herz DM, Cheeran B, Green AL, Fitzgerald J, Aziz TZ, Hyam J, Little S, Foltynie T, et al. (2017). Subthalamic nucleus gamma activity increases not only during movement but also during movement inhibition. Elife 6, 1–21.

Hartmann-Von Monakow K, Akert K, and Kiinzle H (1978). Projections of the precentral motor cortex and other cortical areas of the frontal lobe to the subthalamic nucleus in the monkey. Exp. Brain Res 33, 395–403. [PubMed: 83239]

Hartmann CJ, Hirschmann J, Vesper J, Wojtecki L, Butz M, and Schnitzler A (2018). Distinct cortical responses evoked by electrical stimulation of the thalamic ventral intermediate nucleus and of the subthalamic nucleus. Neuroimage Clin 20, 1246–1254. [PubMed: 30420259]

Haynes WIA, and Haber SN (2013). The organization of prefrontal-subthalamic inputs in primates provides an anatomical substrate for both functional specificity and integration: implications for basal ganglia models and deep brain stimulation. J. Neurosci 33, 4804–4814. [PubMed: 23486951]

Horn A, and Kühn AA (2015). Lead-DBS: a toolbox for deep brain stimulation electrode localizations and visualizations. Neuroimage 107, 127–135. [PubMed: 25498389]

Houde JF, and Nagarajan SS (2011). Speech production as state feedback control. Front. Hum. Neurosci 5, 1–14. [PubMed: 21283556]

Kelly RM, and Strick PL (2004). Macro-architecture of basal ganglia loops with the cerebral cortex: use of rabies virus to reveal multisynaptic circuits. Prog. Brain Res 143, 447–459.

Kolomiets BP, Deniau JM, Mailly P, Mé Né Trey A, Glowinski J, and Thierry AM (2001). Segregation and convergence of information flow through the cortico-subthalamic pathways. J. Neurosci 21, 5764–5772. [PubMed: 11466448]

Kumaravelu K, Oza CS, Behrend CE, Grill WM, Kumaravelu K, Oza CS, Behrend CE, and Grill WM (2018). Model-based deconstruction of cortical evoked potentials generated by subthalamic nucleus deep brain stimulation. J. Neurophysiol 120, 662–680. [PubMed: 29694280]

Kunzle H (1978). An autoradiographic analysis of the efferent connections from premotor and adjacent prefrontal regions (areas 6 and 9) in Macaca fascicularis. Brain Behav. Evol 15, 210–234.

Kuriakose R, Saha U, Castillo G, Udupa K, Ni Z, Gunraj C, Mazzella F, Hamani C, Lang AE, Moro E, et al. (2010). The nature and time course of cortical activation following subthalamic stimulation in Parkinson's disease. Cereb. Cortex 20, 1926–1936. [PubMed: 20019146]

Lai C, Fisher S, Hurst J, Vargha-Khadem F, and Monaco A (2001). A forkhead-domain gene is mutated in a severe speech and language disorder. Nature 413, 519–522. [PubMed: 11586359]

Lardeux S, Paleressompoulle D, Pernaud R, Cador M, and Baunez C (2013). Different populations of subthalamic neurons encode cocaine vs. sucrose reward and predict future error. J. Neurophysiol 110, 1497–1510. [PubMed: 23864369]

Lau B, Monteiro T, and Paton JJ (2017). The many worlds hypothesis of dopamine prediction error: implications of a parallel circuit architecture in the basal ganglia. Curr. Opin. Neurobiol 46, 241–247. [PubMed: 28985550]

Lee PS, Weiner GM, Corson D, Kappel J, Chang Y-F, Suski VR, Berman SB, Homayoun H, Van Laar AD, Crammond DJ, et al. (2018). Outcomes of interventional-MRI versus microelectrode recording-guided subthalamic deep brain stimulation. Front. Neurol 9, 1–8. [PubMed: 29403429]

Lieberman P (2009). FOXP2 and human cognition. Cell 137, 800–802. [PubMed: 19490887]

Lipski WJ, Wozny TA, Alhourani A, Kondylis ED, Turner RS, Crammond DJ, and Richardson RM (2017). Dynamics of human subthalamic neuron phase-locking to motor and sensory cortical oscillations during movement. J. Neurophysiol 118, 1472–1487. [PubMed: 28592690]

Magill PJ, Sharott A, Bevan MD, Brown P, and Bolam JP (2004). Synchronous unit activity and local field potentials evoked in the subthalamic nucleus by cortical stimulation. J. Neurophysiol 92, 700–714. [PubMed: 15044518]

Mallet L, Schüpbach M, N'Diaye K, Remy P, Bardinet E, Czernecki V, Welter ML, Pelissolo A, Ruberg M, Agid Y, et al. (2007). Stimulation of subterritories of the subthalamic nucleus reveals its role in the integration of the emotional and motor aspects of behavior. Proc. Natl. Acad. Sci. U. S. A 104, 10661–10666. [PubMed: 17556546]

Mathai A, and Smith Y (2011). The corticostriatal and corticosubthalamic pathways: two entries, one target. So what? Front. Syst. Neurosci 5, 1–10. [PubMed: 21347218]

Middleton FA, and Strick PL (2000). Basal ganglia and cerebellar loops: motor and cognitive circuits. Brain Res. Rev 31, 236–250. [PubMed: 10719151]

Miocinovic S, de Hemptinne C, Chen W, Isbaine F, Willie JT, Ostrem JL, and Starr PA (2018). Cortical potentials evoked by subthalamic stimulation demonstrate a short latency hyperdirect pathway in humans. J. Neurosci 38, 9129–9141. [PubMed: 30201770]

Mosher CP, Mamelak AN, Malekmohammadi M, Pouratian N, and Rutishauser U (2020). Distinct roles of dorsal and ventral subthalamic neurons in action selection and cancellation. Preprint at bioRxiv. 10.1101/2020.10.16.342980.

Nambu A, Takada M, Inase M, and Tokunoz H (1996). Dual somatotopical representations in the primate subthalamic nucleus: evidence for ordered but reversed body-map transformations from the primary motor cortex and the supplementary motor area. J. Neurosci 16, 2671–2683. [PubMed: 8786443]

Nambu A, Tokuno H, and Takada M (2002). Functional significance of the corticosubthalamopallidal hyperdirect pathway. Neurosci. Res 43, 1–7. [PubMed: 12074836]

Obeso JA, Rodríguez-Oroz MC, Benitez-Temino B, Blesa FJ, Guridi J, Marin C, and Rodriguez M (2008). Functional organization of the basal ganglia: therapeutic implications for Parkinson's disease. Mov. Disord 23, 548–559.

Randazzo MJ, Kondylis ED, Alhourani A, Wozny TA, Lipski WJ, Crammond DJ, and Richardson RM (2016). Three-dimensional localization of cortical electrodes in deep brain stimulation surgery from intraoperative fluoroscopy. Neuroimage 125, 515–521. [PubMed: 26520771]

Siman-Tov T, Granot RY, Shany O, Singer N, Hendler T, and Gordon CR (2019). Is there a prediction network? Meta-analytic evidence for a cortical-subcortical network likely subserving prediction. Neurosci. Biobehav. Rev 105, 262–275. [PubMed: 31437478]

Thomas C, Ye FQ, Irfanoglu MO, Modi P, Saleem KS, Leopold DA, and Pierpaoli C (2014). Anatomical accuracy of brain connections derived from diffusion MRI tractography is inherently limited. Proc. Natl. Acad. Sci. U. S. A 111, 16574–16579. [PubMed: 25368179]

Turner RS, and Desmurget M (2010). Basal ganglia contributions to motor control: a vigorous tutor. Curr. Opin. Neurobiol 20, 704–716. [PubMed: 20850966]

Ullman M (2006). Is Broca's area part of a basal ganglia thalamocortical circuit? Cortex 42, 480–485. [PubMed: 16881254]

Walker HC, Huang H, Gonzalez CL, Bryant JE, Killen J, Cutter GR, Knowlton RC, Montgomery EB, Guthrie BL, and Watts RL (2012). Short latency activation of cortex during clinically effective subthalamic deep brain stimulation for Parkinson's disease. Mov. Disord 27, 864–873. [PubMed: 22648508]

Winer JA (2006). Decoding the auditory corticofugal systems. Hear. Res 212, 1–8. [PubMed: 16555378]

Highlights

- Evoked potentials are used to map the human basal ganglia hyperdirect pathway

- The inferior frontal gyrus appears directly connected to the subthalamic nucleus

- The superior temporal gyrus appears directly connected to the subthalamic nucleus

- Speech perception and planning cortex connect directly to the subthalamic nucleus
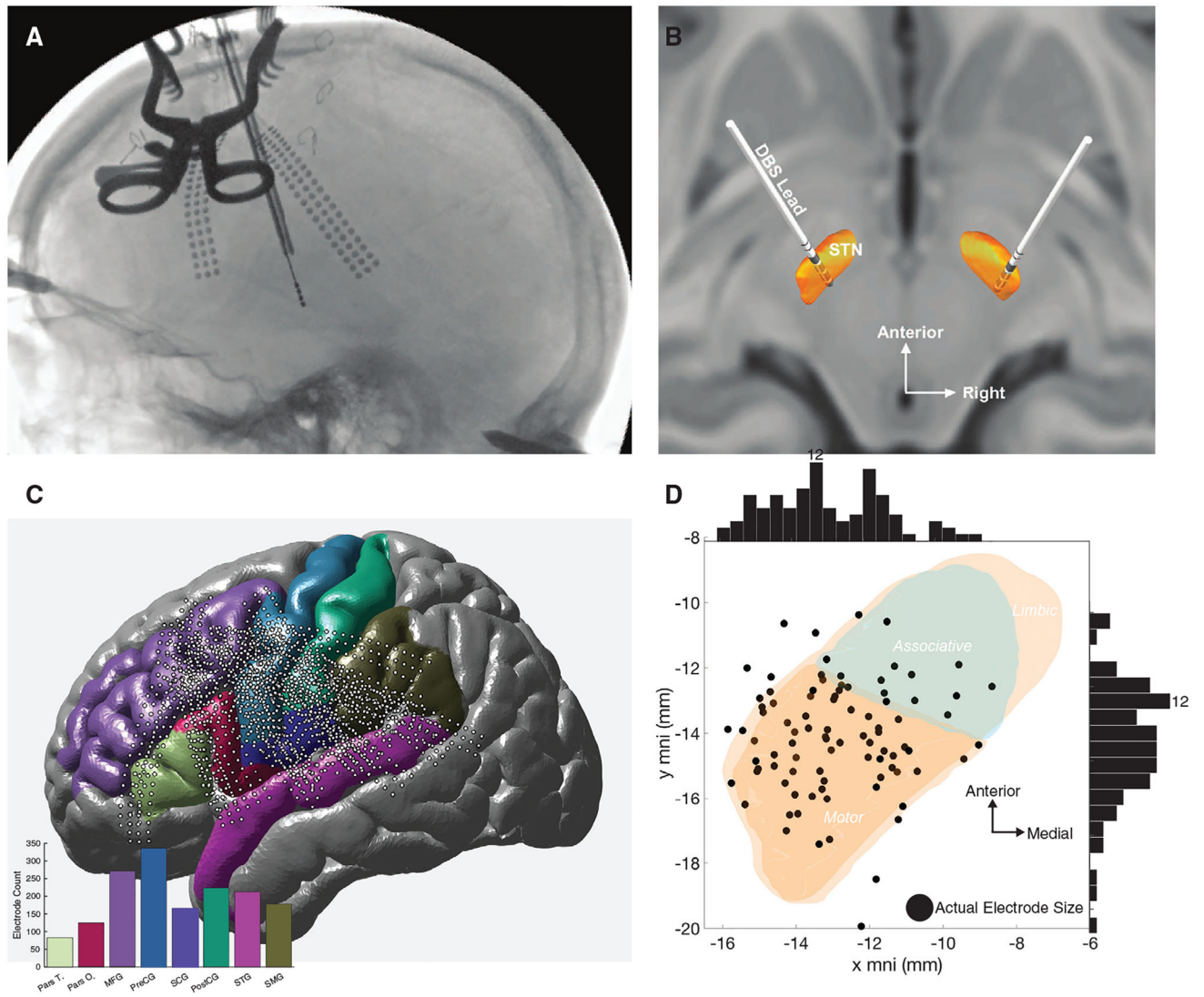
Figure 1. Experimental design

(A) Representative intraoperative fluoroscopy imaging performing during surgery to localize ECoG electrodes on the cortex.

(B) Representative STN DBS localization.

(C) All ECoG electrode locations (black circle dots) with an inset histogram count of all electrodes per cortical area of interest.

(D) All stimulation contact locations (black circle dots) within the left STN, and sideline histograms highlight location distribution; coordinate axes as specified in the Lead-DBS MNI ICBM atlas, where x specifies the mediolateral and y specifies the anteroposterior direction.
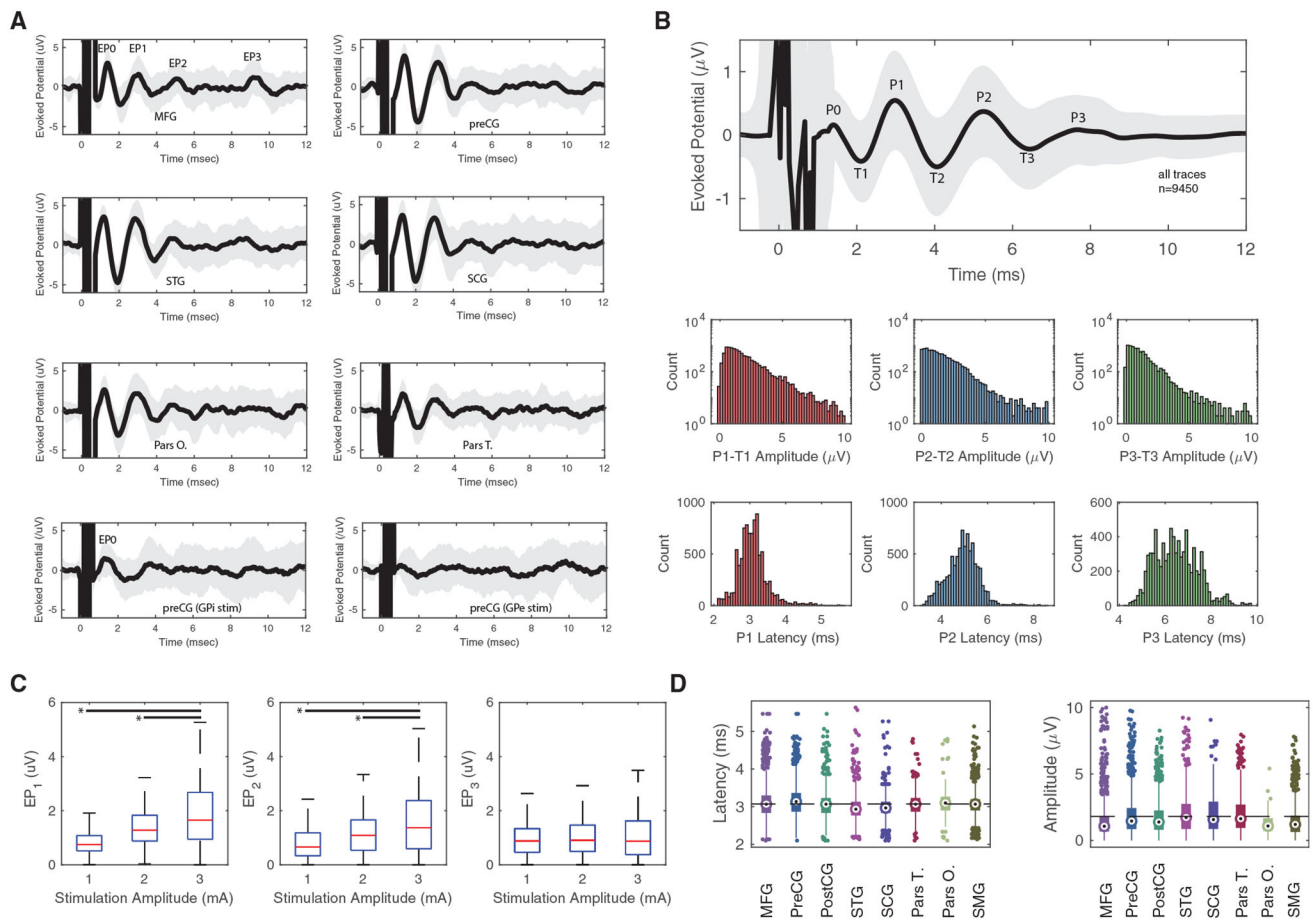
Figure 2. Characterization of cortical EPs

(A) Examples of 3 mA STN (top six subpanels) and GP (bottom two subpanels) stimulation in a single subject for different brain gyri. GPi stimulation elicited an EP0 consistent with its proximity to the internal capsule but no appreciable EP1–EP3. GPe stimulation elicited no EPs. The thick black line and the gray region correspond to the mean and standard deviation, respectively, of the cortical EP of 30 stimulation trials for one subject and one stimulation location. Stimulation occurred at time 0. EP0 corresponds to the peak associated with very short EPs, while EP1–EP3 corresponds to the peaks involved with the hyperdirect pathway.

(B) Top panel: averaged EP peaks (P) and throughs (T) after STN stimulation for all traces. Mean is presented as a black line, and standard deviation is presented as a gray shadow. Bottom panels: amplitude and latency distribution of the difference between peaks and troughs for EP1–EP3.

(C) EP amplitude changes are plotted with interquartile ranges as a function of stimulation amplitude for different EP peaks. *, significant difference in an ANOVA test.

(D) EP1 latency and amplitude distribution plotted as a function of cortical area for latency and amplitude for all traces. Circle represents median, rectangle represents 25–75 quantiles, and the thin line represents upper and lower quartiles.
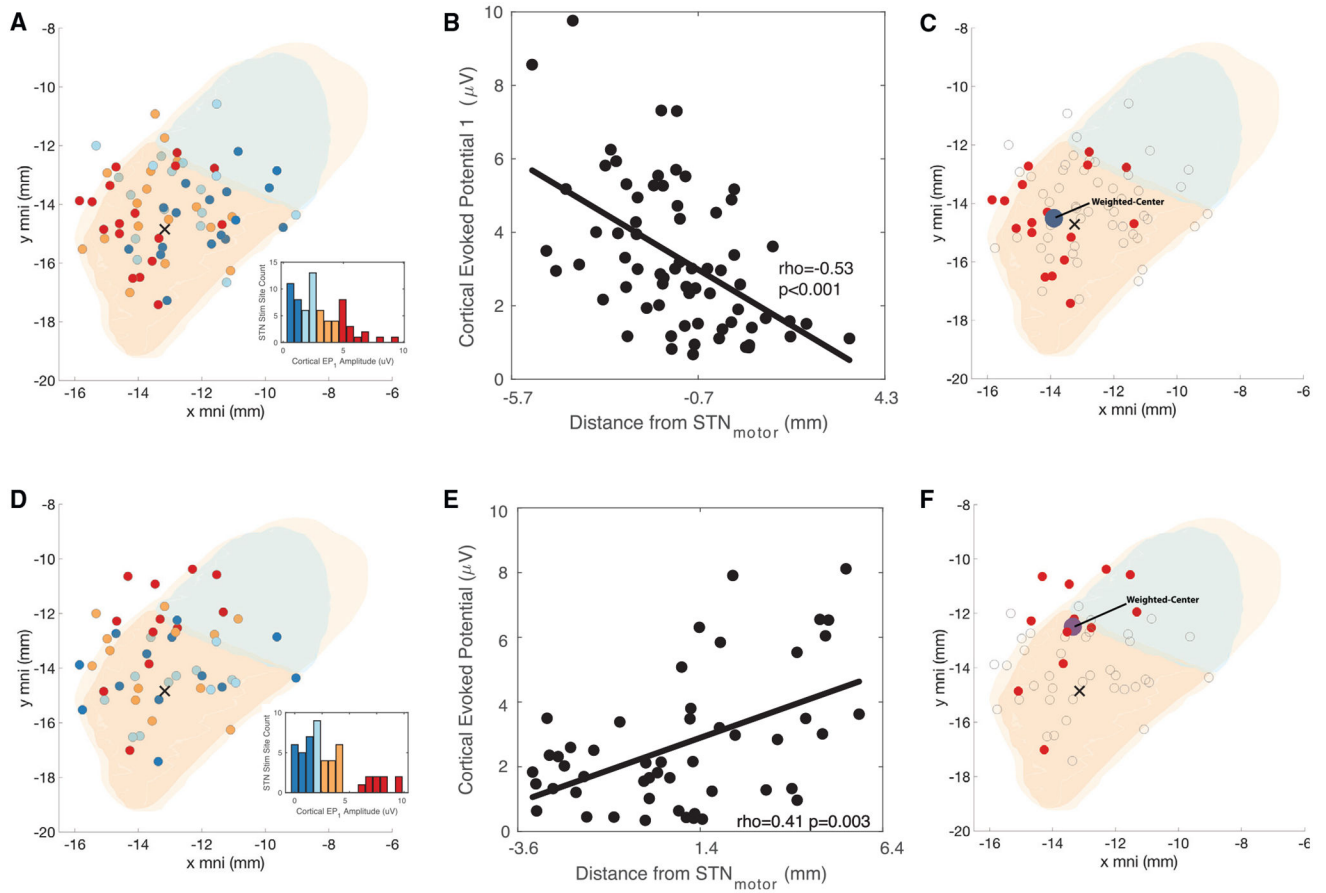
Figure 3. Cortical EPs projected onto the STN

(A–E) Average values from all cortical recording sites in each region were averaged to one single value and plotted on each STN stimulation site for the precentral gyrus (A–C) and the middle frontal gyrus (D–E).

(A) Individual STN stimulation site and projected average precentral gyrus cortical EP in color representing interquartile voltage measures (dark blue, 1st quantile, light blue, 2nd quantile, orange, 3rd quantile, and red, 4th quantile; x represents the center of motor STN).

(B) All precentral gyrus cortical EP projected onto the defined one-dimensional STN axis.

(C) Weighted center of EP response for the upper quartile of precentral cortical EPs.

(D–F) Similar representations as previous panels but projecting the cortical EP from the MFG. The motor aspect of the STN is colored in orange, associative in green, and limbic in yellow, in panels (A), (C), and (D), respectively.

(F) Some points are outside the STN because representation in group space can distort the relation to the patient specific anatomy, and some contacts are outside of the STN. The diameter of each microelectrode tract at the level of the stimulation contact is 1.27 mm.
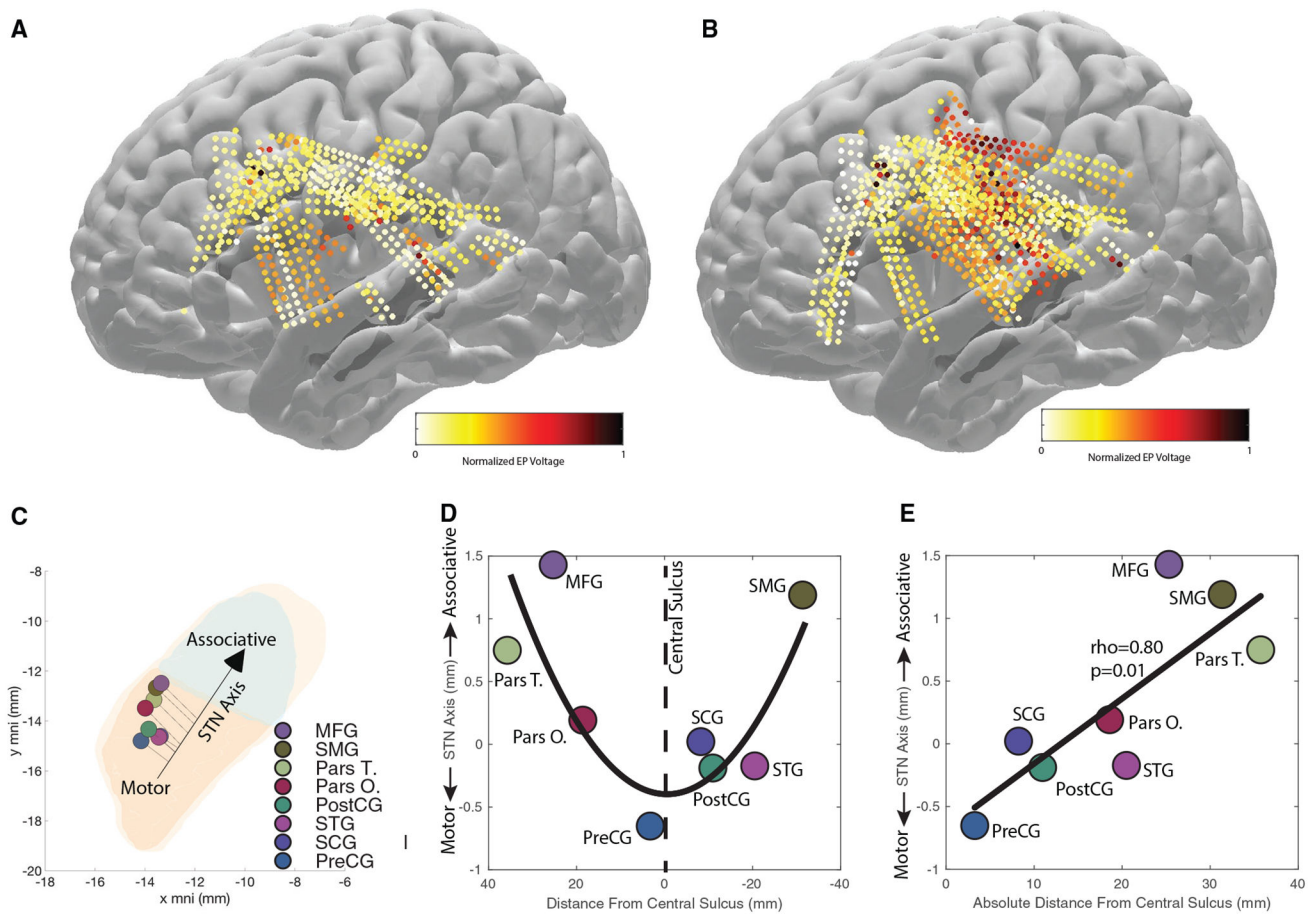
Figure 4. EP amplitude as a function of STN stimulation location

(A) EP amplitude for STN stimulations closer to the STN associative center (the quantile containing the most frontomedial stimulation locations in the STN).

(B) EP amplitude for STN stimulations closer to the STN motor center (the quantile containing the most posterolateral stimulation locations in the STN). Electrodes that did not show an EP are not shown.

(C) Weighted center of cortical EP in the STN per cortical area, and motor aspects of the STN are colored in orange, associative in green, and limbic in yellow. A correlation between stimulation locations along the STN and recording locations along the cortex was found (D) that we simplified, due to the complex geometry, with a linear model of the absolute distance from the central sulcus on the cortical surface of the brain (E).

(D) The quadratic relationship between the STN center of voltage and the corresponding cortical location on the y MNI axis ($p = 0.003$).

(E) The linear model results depicting a significant relationship between STN center of voltage and the absolute distance from the central sulcus ($p = 0.01$).

KEY RESOURCES TABLE

REAGENT or RESOURCE	SOURCE	IDENTIFIER
Deposited data		
Electrophysiological data	This paper.	https://doi.org/10.7910/DVN/CNI25V
Analysis code	This paper.	https://doi.org/10.5281/zenodo.5932678 https://zenodo.org/record/5932678#.Yfhus2BOkh8
Software		
MATLAB	Mathworks, Natick, MA	https://www.mathworks.com/products/matlab.html
Lead-DBS	Charité University Medicine, Berlin, Germany.	https://www.lead-dbs.org